2990, 1260 (P=O, s), 1050-1025 (vs), 965 cm^{-1}; Mass (m/e, %) 91 (100), 260 (53.3), 382 (M, 0.52).

Diethyl 4-methylphenylthio(n-propylthio)methanephosphonate (4f). ^1H NMR ($CDCl_3$) δ 0.92 (3H, t), 1.28 (6H, t), 1.58 (2H, m), 2.28 (3H, s), 2.80 (2H, t), 3.95 (1H, d), 4.13 (4H, dq), 7.00-7.50 (4H, m); IR ($CHCl_3$) 1260 (P=O, s), 1055-1030 (vs) cm^{-1}.

Diethyl isopropylthio(4-methylphenylthio)methanephosphonate (4g). ^1H NMR ($CDCl_3$) δ 1.28 (6H, d), 1.35 (6H, t), 2.33 (3H, s), 3.33 (1H, m), 3.93 (1H, d), 4.17 (4H, dq), 7.00-7.53 (4H, m); IR ($CHCl_3$) 1260 (P=O, s), 1055-1030 (vs) cm^{-1}; Mass (m/e, %) 91 (29.0), 127 (59.0), 155 (54.2), 183 (100.0), 225 (47.0), 274 (32.0), 348 (M, 4.6).

Diethyl 4-methylphenylthio(phenylthio)methanephosphonate (4h). ^1H NMR ($CDCl_3$) δ 1.30 (6H, t), 2.30 (3H, s), 4.17 (4H, dq), 4.27 (1H, d), 6.93-7.53 (9H, m); IR ($CHCl_3$) 1260 (P=O, s), 1050-1025 (vs) cm^{-1}.

References

1. Maryanoff, B. E.; Reitz, A. B. *Chem. Rev.* **1989**, *89*, 863.
2. Mastalerz, P. In *Handbook of Organophosphorus Chemistry*; Engel, R., Ed.; Marcel dekker, Inc.: New York, U.S.A., 1992; Chapter 7.
3. (a) Kim, T. H.; Oh, D. Y. *Tetrahedron Lett.* **1986**, *27*, 1165. (b) Kim, T. H.; Oh, D. Y. *Synth. Commun.* **1988**, *18*, 1611.
4. (a) Kim, T. H.; Kim, D. Y.; Oh, D. Y. *Synth. Commun.* **1987**, *17*, 755. (b) Kim, T. H.; Oh, D. Y. *Synth. Commun.* **1994**, *24*, 2313.
5. Mikolajczyk, M.; Grejszczak, S.; Chefczynska, A.; Zatorski, A. *J. Org. Chem.* **1979**, *44*, 2967.
6. Mikolajczyk, M.; Balczewski, P.; Grejszczak, S. *Synthesis* **1980**, 127.
7. Kim, D. Y.; Kim, T. H.; Oh, D. Y. *Phosphorus and Sulfur* **1987**, *34*, 179.
8. (a) Arbusov reaction of phosphites with chlorodithioacetals; Blotkowska, B.; Gross, H.; Costisella, B.; Mikolajczyk, M.; Grzejszczak, S.; Zatorski, A. *J. Prakt. Chem.* **1977**, *319*, 17. (b) addition of disulfides to methanephosphonate carbanions; Mikolajczyk, M.; Grzejszczak, S.; Chefczynska, A.; Zatorski, A. *J. Org. Chem.* **1979**, *44*, 2967. (c) reaction of diethoxymethanephosphonate with thiols; Gross, H.; Keitel, I.; Costisella, B.; Mikolajczyk, M.; Midura, W. *Phosphorus and Sulfur* **1983**, *16*, 257. (d) treatment of chloro(arylthio)methanephosphonate with thiols in the presence of Lewis acids.[3b]
9. Ishibashi, H.; Sato, T.; Irie, M.; Ito, M.; Ikeda, M. *J. Chem. Soc., Perkin Trans. 1* **1987**, 1095.
10. Tamura, Y.; Choi, H. D.; Shindo, H.; Uenishi, J.; Ishibashi, H. *Tetrahedron Lett.* **1981**, *22*, 81.
11. We[4a] and Stamos reported that only a para-isomer was obtained in the reaction of **2a** with toluene, isobutylbenzene, cumene, and *ter*-butylbenzene. Stamos, I. *Tetrahedron Lett.* **1986**, *27*, 6261.
12. Green, M. *J. Chem. Soc.* **1963**, 1324.
13. Mikolajczyk, M.; Zatorski, A. *Synthesis* **1973**, 669.

Effect of Carrier Solutions on Particle Retention in Flow Field-Flow Fractionation

Myeong Hee Moon

Department of Chemistry, Kangnung National University, Kangnung 210-702, Korea

Received March 11, 1995

The influence of carrier solutions on particle retention was studied by varying surfactants and ionic strength in flow field-flow fractionation. Experiments were made with five different submicron polystyrene latex standards at three different types of surfactants and seven different ionic strengths. Departures in particle retention from the general theory were observed. At low ionic strength, it is shown that migrating sample zone is clearly lifted away from the ideal equilibrium height and that the repulsive interaction dominates between the particle and the channel wall. As ionic strength increases up to a certain level, particle retention becomes closer to the general theory. Further increase in ionic strength is shown to prolong the retention. An optimum regime of ionic strength is also suggested with the proper choice of surfactants.

Introduction

Field-flow fractionation, a group of separation techniques, is capable of separating and characterizing colloids, polymers, and biological macromolecules.[1~4] FFF techniques utilize external fields (or driving forces) to retain sample components in the separation channel (columns in chromatographic system). Separation in FFF systems is carried out in a thin ribbon-like channel under the application of an external field in the direction perpendicular to the axis of separation flow.[2] The external forces drive sample materials toward the one side of the channel wall (called as accumulation wall) and push the components of different mass or size to distribute at different streampaths of longitudinal flow. The flow moving through the thin channel assumes a laminar type having a parabolic flow profile in which flow velocity is close to

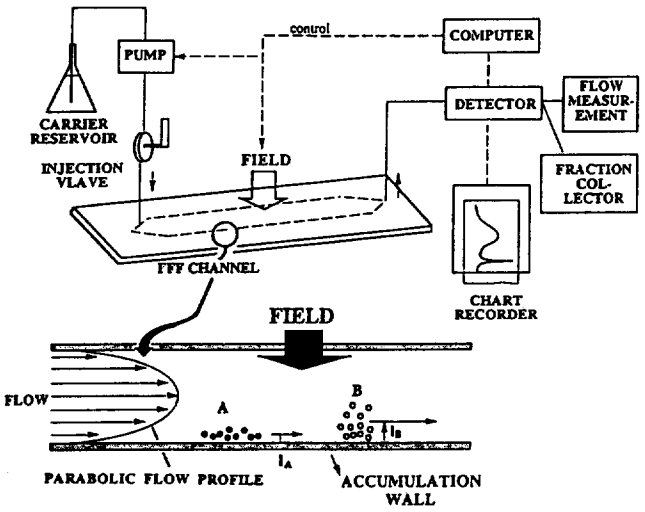

Figure 1. The basic structure of an FFF system with an enlarged edge view of channel illustrating the elution profiles of two different components under the external field.

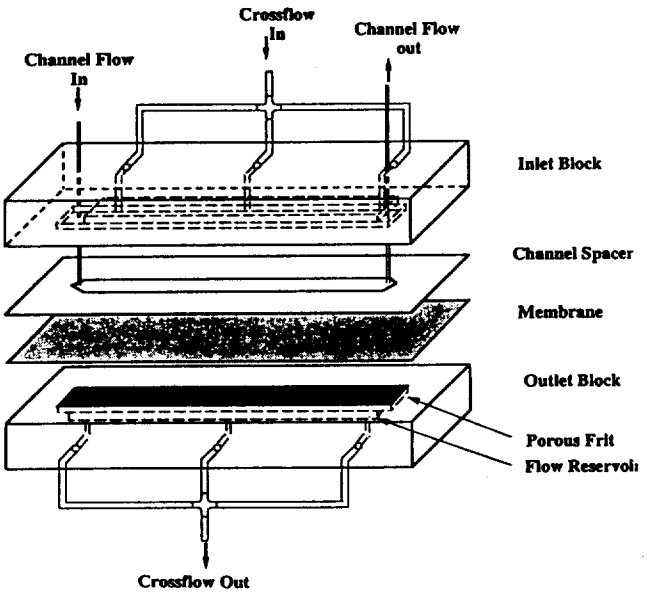

Figure 2. Schematic diagram of flow FFF channel assembly.

zero at the wall and maximum at the center flowstream. This causes unequal moving velocities of the components having different physical characteristics and leads to the separation. Sample components distributed at different flowstreams will be differentially displaced downstream toward the end of the channel and a detector. The principles of FFF are illustrated in Figure 1 with the diagram of basic structure of an FFF system. In the enlarged edge view of channel at Figure 1, samples having different properties represented as *A* and *B* are distributed at different heights, denoted as mean layer thickness, *l*.

Depending on the types of external fields, FFF methods are classified into each subtechnique such as flow FFF, sedimentation FFF, thermal FFF, and electrical FFF.[1~3] Each field is specifically applied for separating various macromolecular species; sedimentation[5,6] for colloids and particulate materials, thermal[7,8] for polymers, and electrial[9] for charged macromolecules. Flow FFF utilizes crossflow as a means of driving force which is recently gaining its versatility in the characterization of broad size range of macromolecules[10~14]; biological materials such as proteins and DNA, synthetic water soluble polymers, and colloids as well. In flow FFF, two permeable ceramic frits are used as a wall material in order to transfer crossflow to and from the channel and the same carrier liquid used as separation flow is delivered to the crossflow inlet by a secondary pump. Mechanical aspect of flow FFF channel is drawn in Figure 2. Permeable membrane, an essential part of flow FFF, is located at the bottom wall of the channel to keep sample materials from penetrating through the frit. The pore size of membrane, of course, is also a point of consideration since sample materials must retain in the channel without loss during FFF operation. When sample components are injected to the flow FFF channel, they are swept by crossflow and remain confined near the accumulation wall. This stage is so called an steady state equilibrium which is achieved by the balance of the inherent Brownian diffusion of sample components and the driving force which suppresses this random motion. When the external field is applied, a large diameter particle or high MW polymer will generally experience a stronger field and approaches closely to the accumulation wall at equilibrium. A component of small size having a relatively rapid diffusion compared to the large one, will be located at a relatively high elevation. Therefore, the small particle will be migrated to the end of the channel by a fast flowstream and eluted earlier than the large one. One of the great advantages in FFF techniques is the possibility of theoretical prediction of particle retention in the channel if the particle size, accurate flowrate of both principal and crossflow are provided. From this relationship, it is possible to calculate particle size or hydrodynamic radius and particle size distribution of polydisperse particulate materials once a proper experimental condition is chosen.

There are some experimental factors governing ideal retention in flow FFF such as optimum flowrate conditions, membrane properties, and carrier solutions. Among these, carrier liquid plays an important role in supporting an ideal model of retention. Since colloids are charged by nature, they are subjected to electrostatic interactions. In case of colloidal particulates translating slightly apart from an FFF channel wall, they are involved with the interactions between particles and the channel wall as well as among particles. There exists a certain discrepancy between theoretical and experimental retention values which are often affected by the ionic strengths and type of surfactants. Earlier reports[15,16] on this retention perturbation are mainly focused on sedimentation FFF works which suggest particle-wall interactions either attractive or repulsive influence the retention of particles in sedimentation FFF.

In this paper, retention behavior of polystyrene particles in flow FFF is experimentally examined by varying ionic strengths of carrier liquid with different kinds of surfactants. In solutions of low ionic strength, particles are expected to have high repulsive interactions from the wall, and are predicted to form a diffused sample zone located far away from the wall. This will result in the decrease of particle retention

and thus in the departure from the theory. Effect of surfactants, generally used for improving sample dispersion and for preventing sample adsorption from the channel wall, is examined with the optimum range of concentration. Theory Retention theory of most polymers and colloidal materials in flow field-flow fractionation has been developed and discussed in a number of reports.[6,11,17] In flow FFF, general equation for retention time, t_r, of a given component is expressed by

$$t_r = \frac{t^o}{6\lambda\left(\coth\left(\frac{1}{2\lambda}\right) - 2\lambda\right)} \quad (1)$$

where t^o is the void time, the passage time of the non-retained materials, and λ is the retention parameter which is a basic FFF parameter determined from the characteristics of the sample components to be separated. The retention parameter, λ, which is dimensionless and defined as the ratio of mean layer thickness of sample zone, l, to the channel thickness, w, (see Figure 1) is dependent on the applied field strength, F, as

$$\lambda = \frac{l}{w} = \frac{kT}{Fw} \quad (2)$$

where kT is the thermal energy. The applied field strength, F, acts as a driving force to push the sample components toward the accumulation wall (bottom wall) from the top side of the channel. This force is given by

$$F = kT\frac{U}{D} \quad (3)$$

where U is the field induced drifting velocity of the sample component across the channel by the cross-flow and D is the diffusion coefficient. Thus, separation in flow FFF is based on the differences in D of sample materials. Diffusion coefficient in Eq. (3) is related to the Stoke's diameter, d_s, of the components by[11]

$$D = \frac{kT}{3\pi\eta d_s} \quad (4)$$

where is the viscosity of carrier liquid. When the field induced drifting velocity, U, is written in terms of volumetric flowrate of cross-flow, $\dot{V}_c$ the field strength in flow FFF becomes

$$F = \frac{3\pi\eta d_s \dot{V}_c}{bL} \quad (5)$$

where b is the channel breadth and L is the channel length.

When particle retention in FFF is sufficiently long enough to achieve an efficient operation, Eq. (1) can be simply reduced as

$$t_r \cong \frac{t^o}{6\lambda} \qquad \text{(when } \lambda \text{ is very small)} \quad (6)$$

The void time, t^o, can be written as the geometric channel volume divided by the channel flowrate, $\dot{V}$, as

$$t^o = \frac{bwL}{\dot{V}} \quad (7)$$

From Eqs. 2, 5, and 7, retention time in Eq. (6) can be finally expressed as follows

$$t_r = \frac{\pi\eta w^2}{2kT}\,\frac{\dot{V}_c}{\dot{V}}\,d_s \quad (8)$$

According to the above equation, retention time, t_r, is approximately proportional to Stoke's diameter, d_s, the ratio of cross flowrate to channel flowrate, and the square of the channel thickness. Thus, theoretical prediction of particle retention can be obtained once proper experimental conditions are selected and likewise, particle size can also be calculated from the measured retention time.

Experimental

The flow FFF system used in this study is a model F1000 Universal Fractionator from FFFractionation, Inc. (Salt Lake City, UT, USA). The flow FFF channel assembly is schematically shown in Figure 2. The channel dimension has a tip to tip length, L, of 27.2 cm and a breadth, b, of 2.00 cm. The channel space is made of a 178 μm thick Mylar sheet cut as a ribbonlike structure. Due to the compression of the membrane by the spacer when they are assembled, the effective channel thickness was reduced to 157 μm measured from the channel void volume, 0.79 mL, by the rapid breakthrough method.[18] The membrane used throughout the study is YM-30, a regenerated cellulose having cut-off pore size of MW 30,000 made by Amicon (Beverly, MA, USA). The backside of the membrane used in this work was treated with silicon glue specially for flow FFF run in this lab by pasting thin layer of glue around the edge (excluding the channel space region) in order to keep channel from leaking.

Sample materials used in this work are the polystyrene latex standards with nominal size of 0.091, 0.105, 0.173, 0.220, and 0.304 μm in diameter from Duke Scientific (Palo Alto, CA, USA). The standard solutions are diluted 200-400 times with reverse osmotically purified and deionized water containing 0.05% (w/v) SDS (sodium dodecylsulfate) for particle dispersion and 0.02% NaN_3 as a bactericide.

Carrier liquids for the separation of standards in flow FFF are made with the same pure water and a proper surfactant and salt. Surfactants used in the study are SDS (anionic), FL-70 (a mixture of anionic and nonionic surfactants) from Fisher Scientific (Fairlawn, NJ, USA), and Triton X-100 (nonionic) from E. Merck (Darmstadt, Germany). Experiments are carried out by measuring the retention times of standard particles under different concentrations of these surfactants, and NaN_3 as a source of salt in carrier liquids. For the delivery of carrier liquid into the channel through two inlets, one for channel flow and the other for crossflow, two Waters 510 HPLC pumps from Waters (Milford, MA, USA) were used. Sample materials were injected onto the flowstream by a model 7125 loop injector from Rheodyne (Cotati, CA, USA). Injection volume of each standard is about 1-2 μL of the diluted sample solution. The regular stopflow method in which the channel flow is regularly halted right after sample injection is used to achieve "relaxation", a process to provide steady-state equilibrium for particles above the channel wall, before separation begins. The calculated stopflow periods are 1-2 minutes, the time necessary to sweep one channel void volume across the channel by crossflow, depending on the cross flowrates used in each run. The eluted

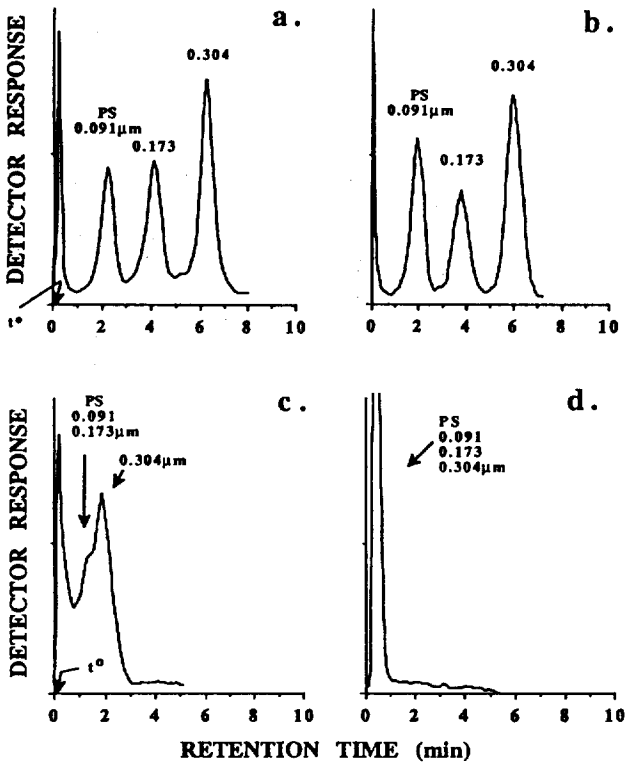

Figure 3. Separation of polystyrene standards (diameters shown inside) obtained at different carrier solutions; a) 0.05% SDS with 0.02% NaN_3, b) 0.1% FL-70 with 0.02% NaN_3, c) 0.1% Triton X-100 with 0.02% NaN_3, and d) pure water. The experimental condition for all runs is $\dot{V}=7.17$, $\dot{V}_c=1.09$ mL/min.

polystyrene standards were monitored right after the channel outlet by a model 720 absorbance detector from Young-In Scientific (Seoul, Korea) at a wavelength of 254 nm and recorded by a model E586 Labograph chart recorder from Metrohm (Herisau, Switzerland).

Results and Discussion

Figure 3 shows the comparison of fractograms of polystyrene standards obtained at different carrier solutions in flow FFF. The run conditions for all runs are the same as a channel flowrate of 7.17 mL/min and a cross flowrate of 1.09 mL/min. The fractogram in Figure 3a is a typical separation of submicron polystyrene latex spheres with a high resolving power. This run was obtained with a carrier solution containing 0.05% SDS, an anionic surfactant, with 0.02% NaN_3 as a bactericide. When 0.1% FL70, a mixture of anionic and nonionic type of surfactant, is used instead of SDS, a good resolution is achieved except for the slight decrease in retention time scale in Figure 3b. These two surfactants are commonly used in most flow FFF operations to resolve particulate materials since the use of surfactant improves the dispersion of particles and keeps them from aggregating each other. When pure water is used as a carrier liquid without adding surfactant or salt, retention behavior of polystyrene particles is unacceptable as in Figure 3c. When ionic strength of carrier solution is close to zero, the electrical double layer becomes thick and prevents particles from getting close to

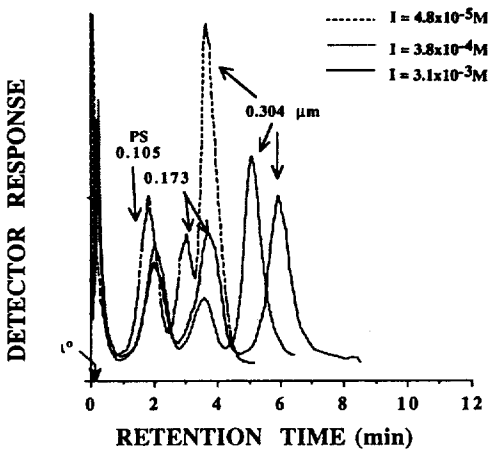

Figure 4. Superimposed fractograms of polystyrene separation at different ionic strength solutions obtained at $\dot{V}=5.65$, $\dot{V}_c=0.75$ mL/min.

the channel wall during the relaxation process due to the double layer repulsion. The electrostatic interactions between particles and the channel wall depend on the ionic strengths of liquid medium. However, when a nonionic surfactant such as Triton X-100 is used in the carrier liquid with the addition of sodium azide, none of the individual peaks are observed at the fractogram in Figure 3d. Standard particles appear to elute all at once along the large single peak, a system transient usually observed at a stopflow run, right after the beginning of the separation. This is somewhat unexpected since the carrier contains the same amount of sodium azide as used in Figure 3a and b. In addition, the original standard particles used for all runs were diluted in the same carrier solution as used in Figure 3a. Therefore, there should be no chance of particle aggregation before they are injected. During relaxation process in flow FFF, sample solutions are swept across the channel through the membrane by the crossflow leaving particles in the channel. At this stage, they encounter the nonionic surfactant and seem to be poorly dispersed or be aggregated to a big cluster resulting in a nonretained peak. It is noted that nonionic surfactant might deteriorate particle dispersion inside the channel and that Triton X-100 is not a proper surfactant in flow FFF operation.

For elucidating the effect of ionic strength on particle separation, the same experiments were carried out with different ionic strengths by changing amounts of sodium azide in pure water without adding any surfactant. Figure 4 shows superimposed fractograms of polystyrene standards at three different ionic strengths obtained at a channel flowrate of 5.65 mL/min and a cross flowrate of 0.75 mL/min. When the ionic strength is $I=4.8\times10^{-5}$ M represented as broken line in Figure 4, separation is somewhat improved compared to the fractogram obtained with pure water (see Figure 3c). Individual sample peaks begin to appear upon the slight addition of salt. As the ionic strength increases to $I=3.8\times10^{-4}$ M, each peak clearly shifts to a longer retention time scale and peaks of 0.173 and 0.304 μm particles are completely separated each other. It is demonstrated that the retention time increases when the ionic strength is increased. This implies that particle migration above the wall is made at

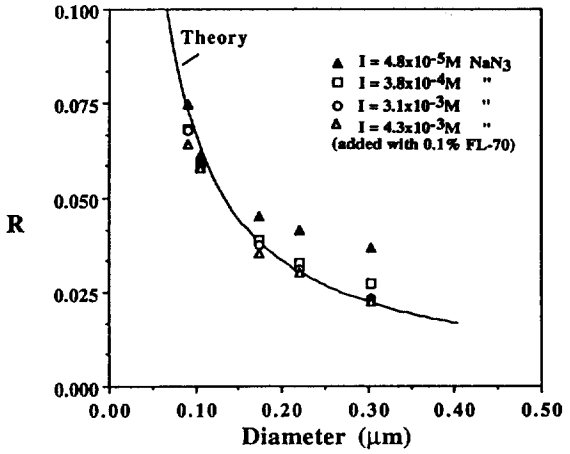

Figure 5. Retention ratio R vs. particle diameter at different ionic strengths. Ionic strengths are varied by the amount of NaN_3. Run conditions are the same as used in Figure 4.

different equilibrium heights depending on the ionic strengths of fluid medium. At a higher ionic strength ($I=3.1\times10^{-3}$ M), a similar resolution is achieved as observed in Figure 3a. It is likely that particles approach closely to the channel wall without severe repulsion from the wall due to the simultaneous decrease in double layer thickness as ionic strength increases. When the ionic strength is increased above 3 mM, there is no significant change in the retention times but a mild increase is observed with similar resolution (not shown in this figure). This implies that there is a certain ionic strength region for an optimum flow FFF operation. In order to examine the deviations in retention time from the theory, the retention ratio (R), defined[6,11,17] as the ratio of void time (t^o) to retention time (t_r), of each peak is plotted against particle diameter in Figure 5. The solid curve in Figure 5 represents the theoretical plot of retention ratio calculated from Eq. (6) and the experimental data are shown as symbols whose ionic strengths are marked inside the figure. At a low ionic strength, particle retention deviates from the theory curve to a great extent as the particle diameter increases. The deviation is induced from the increase of double layer repulsion from the wall at a low ionic strength leading to the elevation of sample layer to a higher flowstream. It results in the decrease in the retention time. This effect decreases when the ionic strength increases to a level of 10^{-3} M. Retention values obtained at $I=3.1\times10^{-3}$ M (plotted as circle) fits the theory curve quite well. When 0.1% FL70 is added to this solution, no significant differences in the retention are observed because the total ionic strength ($I=4.29\times10^{-3}$ M) is not greatly changed compared to the previous run condition. However, the effect of nonionic components of FL-70 surfactant (both anionic and nonionic) does not seem to alter the retention behavior as Triton X-100 solution does.

The departure in particle retention from theory is amplified when a higher cross flowrate is used. The data are not included in this article. When a cross flowrate is increased to 1.09 mL/min with a simultaneous increase in channel flowrate to 7.20 mL/min, it is found that retention of particles deviates further from the theory. It implies that particles

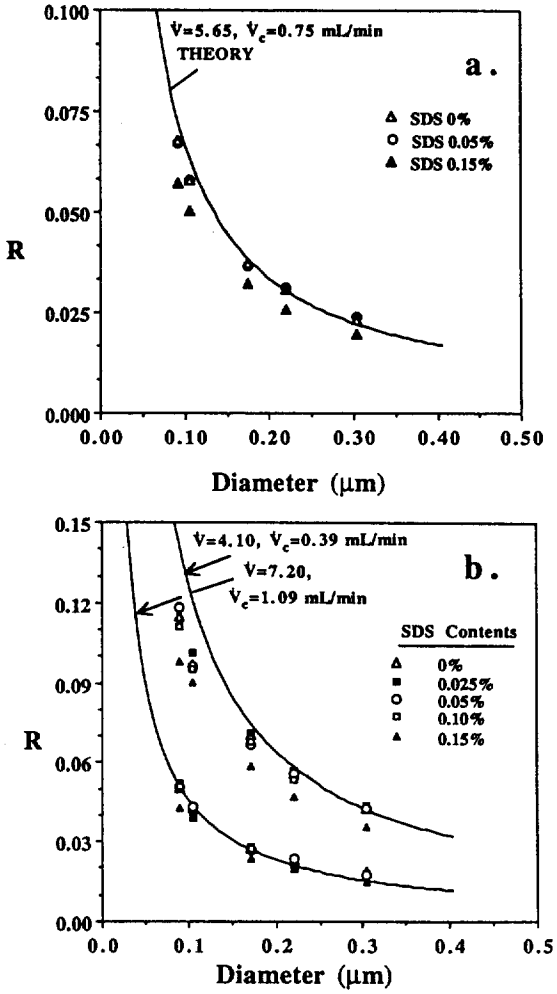

Figure 6. R vs. particle diameter under various SDS concentrations obtained at a) $\dot{V}=5.65$, $\dot{V}_c=0.75$ mL/min, b) $\dot{V}=4.10$, $\dot{V}_c=0.39$ mL/min for the data set at top curve and $\dot{V}=7.20$, $\dot{V}_c=1.09$ mL/min for the lower set. All solutions are containing 0.02% NaN_3.

under a strong field experience strong repulsive forces since particles are driven closely to the wall. At a mild run condition such as $\dot{V}=4.10$, $\dot{V}_c=0.39$ mL/min, there observed no significant differences in particle retention obtained at different ionic strengths. It represents that particle equilibrium height is relatively high where repulsion from the wall is less dominating.

Influence of surfactants was examined by varying the concentration of SDS while the concentration of sodium azide is fixed to 0.02%. Figure 6a shows the plot of retention ratio vs. particle diameter obtained at three different concentrations of SDS solutions. The run condition is $\dot{V}=5.65$, $\dot{V}_c=0.75$ mL/min. Since all carrier solutions used in this test contain the same amount of sodium azide ($I=3.1\times10^{-3}$ M), retention perturbations would not be as serious as observed in earlier sets of experiment. However, prolonged retention appears as ionic strength increases further. That results in the decrease of retention ratio from the theory curve. It is shown that a certain level of SDS concentration up to 0.05% SDS does not severely alter the retention. The combined

Table 1. Double Layer Thickness at Each Carrier Solution

Surfactants	Salts	Total I (M)	k^{-1} (nm)	Remarks
	0.0003% NaN_3	4.80 E-5	43.96	
	0.0025% 〃	3.84 E-4	15.54	
	0.02% 〃	3.07 E-3	5.49	
0.1% FL-70	〃 〃	4.29 E-3	4.65	Nonionic &
0.2% 〃	〃 〃	5.51 E-3	4.10	Anionic
0.1% Triton X-100	〃 〃	3.07 E-3	5.49	Nonionic
0.02% SDS	〃 〃	3.94 E-3	4.85	Anionic
0.05% 〃	〃 〃	4.87 E-3	4.36	〃
0.10% 〃	〃 〃	6.53 E-3	3.77	〃
0.15% 〃	〃 〃	8.26 E-3	3.35	〃

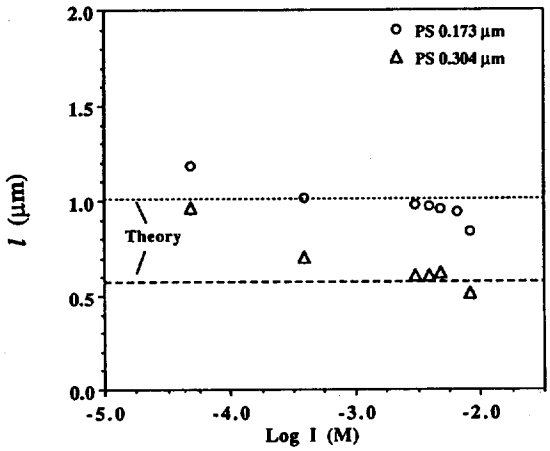

Figure 7. Mean layer thickness l vs. Log I (ionic strength) for two different particle sizes obtained at a same run condition used in Figure 6a.

ionic strength is listed at Table 1. An SDS solution of high concentration (0.15% SDS, I_{tot}=5.19E-3 M) provides delayed retention for particles of all sizes. The deviations in the retention values are about 10-15% from the theory curve. In this case, particle migrations above the accumulation wall seem to happen at a distance even closer than they are expected due to the increase of ionic strength by SDS. When the flowrates are varied, perturbations are somewhat different. Figure 6b compares the differences in R observed in two different run conditions. Retention of particles at a high flowrate condition ($\dot{V}$=7.20, $\dot{V}_c$=1.09 mL/min) is not strongly affected by the addition of SDS compared to the relatively low flowrate runs. The effect of additional increase in ionic strength (from SDS) seems to be less important at a high cross flowrate once a minimum ionic strength is provided in the carrier liquid. Since all carrier solutions contain a reasonable amount of salt (0.02% NaN_3, I=3.07E-3 M) enough for efficient separation, double layer repulsion from the wall is kept minimum. A high cross flowrate appears to suppress the diffusive transport of particles from the wall efficiently. The values of mean layer thickness, l, of two polystyrene standards such as 0.173 and 0.304 μm are plotted against the logarithm of ionic strengths in Figure 7. The dotted lines are the theoretical equilibrium heights for each standard particle, respectively, calculated from Eq. (2) and are compared with the measured data. Figure 7 covers data obtained at all ionic strengths of carrier solutions utilized in this study regardless of the use of surfactant. It is found that data fit to the theory closely at ionic strengths in the range of about I=1-5×10^{-3} M. At a low ionic strength, it is clear that particle's equilibrium height is lifted far away from the channel wall as it is supposed to be. Double layer repulsion at a low ionic strength seems to influence the particle retention since the double layer thickness becomes larger. Double layer thickness at each ionic strength is calculated according to the method of ref. 15 and listed at Table 1. As the ionic strength increases, double layer becomes shrunk and particles are able to approach closer to the channel wall without being interrupted by severe repulsion. Considering the electrostatic repulsive forces and van der Waals attractive forces at or around the electrical double layer, it can be thought that attractive forces are gaining an increasing role when the total ionic strength exceeds I=5×10^{-3} M. The interplay of the two forces at the accumulation wall needs to be systematically examined by comparing the two interactions . Detailed descriptions on particle-wall interaction forces were not provided in this work due to the difficulty in finding the material constants of the membrane needed for the calculation of these forces. However, the current experimental results show a clear evidence of the retention perturbations which are strongly dependent on ionic strength of carrier solutions and this information will be useful in the selection of carrier solutions when the particulate materials are separated in flow FFF.

Conclusions

This study elucidates the effect of carrier solutions (especially ionic strength) on retention perturbations in flow FFF. Specifically, polystyrene latex standards whose diameters range from 0.091 to 0.304 μm are subjected to separation within 10 minutes by flow FFF. Results obtained at different ionic strengths and various surfactants can be utilized for the optimization of flow FFF operation. For ionic strength below I=1×10^{-3} M, an efficient separation could not be obtained due to the strong double layer repulsion from the channel wall. At or above this concentration, retention data fit the theory well until the ionic strength exceeds about I=5×10^{-3} M. At a high ionic strength, it shows a decrease in the mean layer thickness of migrating sample band, which results in the decrease in retention ratio. The use of a nonionic surfactant such as Triton X-100 was not appropriate for the separation of polystyrene latex particles. However, anionic surfactants such as FL-70 and SDS are conducive to the separation of polystyrene standards up to a certain level of concentration where the total ionic strength does not exceed the optimum regime. For the optimization of flow FFF operation much more work is required to investigate these effects in details.

Acknowledgment. The author is grateful to Dr. J. Calvin Giddings and FFFractionation, Inc. for providing a flow FFF channel assembly, to Young-In Scientific for the kind lease of an HPLC pump, and to Mr. Sangbeom Son for the help in lab work. This work was partially supported by Korea Science and Engineering Foundation (951-0304-023-2).

References

1. Giddings, J. C. *Science* **1993**, *260*, 1456.
2. Giddings, J. C. *Chem. Eng. News* **1988**, *66*, 34.
3. Caldwell, K. D. *Anal. Chem.* **1988**, *60*, 959A.
4. Martin, M.; Williams, P. S. In *Theoretical Advancement in Chromatography and Related Separation Techniques*; *NATO ASI Series C Mathematical and Physical Sciences*; Dondi. F.; Guiochon, G. Eds.; Kluwer: Dordrecht, 1992; Vol. 383, p 513.
5. Giddings, J. C.; Yang, F. J. F.; Myers, M. N. *Anal. Chem.* **1974**, *46*, 1917.
6. Giddings, J. C.; Ratanathanawongs, S. K.; Moon, M. H. *KONA: Powder and Particle* **1991**, *9*, 200.
7. Myers, M. N.; Caldwell, K. D.; Giddings, J. C. *Sep. Sci. Technol.* **1974**, *9*, 47.
8. Giddings, J. C.; Hovingh, M. E.; Thomson, G. H. *J. Phys. Chem.* **1970**, *74*, 4291.
9. Caldwell, K. D.; Kesner, L. F.; Myers, M. N.; Giddings, J. C. *Science* **1972**, *176*, 296.
10. Giddings, J. C.; Yang, F. J. F.; Myers, M. N. *Science* **1976**, *193*, 1244.
11. Moon, M. H.; Giddings, J. C. *J. Pharm. Biomed. Anal.* **1993**, *11*, 911.
12. Litzen, A.; Wahlund, K.-G. *J. Chromatogr.* **1989**, *476*, 413.
13. Liu, M. K.; Li, P.; Giddings, J. C. *Protein Science* **1993**, *2*, 1520.
14. Giddings, J. C.; Benincasa, M. A.; Liu, M. K.; Li, P. *J. Liq. Chromatogr.* **1992**, *27*, 1489.
15. Hansen, M. E.; Giddings, J. C. *Anal. Chem.* **1989**, *61*, 811.
16. Moon, M. H.; Williams, P. S.; Giddings, J. C. Unpublished results.
17. Giddings, J. C.; Yang, F. J. F.; Myers, M. N. *Anal. Chem.* **1976**, *48*, 1126.
18. Giddings, J. C.; Williams, P. S.; Benincasa, M. A. *J. Chromatogr.* **1992**, *627*, 23.

Mechanistic Studies on the Oxidation of Triphenylphosphine by $[(tpy)(bpy)Ru^{IV}=O]^{2+}$, Structure of the Parent Complex $[(tpy)(bpy)Ru^{II}\text{-}OH_2]^{2+}$

Won Kyung Seok*†, Mee Yung Kim†, Yoshinobu Yokomori‡, Derek J. Hodgson, and Thomas J. Meyer*§**

†*Department of Chemistry, Dongguk University, Seoul 100-715, Korea*
‡*Department of Chemistry, The National Defence Academy, Hashirimizu, Yokosuka 239, Japan*
**Department of Chemistry, University of Wyoming, Laramie, Wyoming 82071, U.S.A.*
§*Department of Chemistry, The University of North Carolina at Chapel Hill, Chapel Hill, NC 27599-3290, U.S.A.*

Received March 23, 1995

Oxidation of triphenylphosphine to triphenylphosphine oxide by $[(tpy)(bpy)Ru(O)]^{2+}$ (tpy is 2,2′ : 6′,2″-terpyridine and bpy is 2,2′-bipyridine) in CH_3CN has been studied. Experiments with the ^{18}O-labeled oxo complex show that transfer of oxygen from $[(tpy)(bpy)Ru^{IV}=O]^{2+}$ to triphenylphosphine is quantitative within experimental error. The reaction is first order in each reactant with k (25.3 ℃) $=1.25\times10^{6}$ $M^{-1}s^{-1}$. The inital product, $[(tpy)(bpy)Ru^{II}\text{-}OPPh_3]^{2+}$, is formed as an observable intermediate and undergoes slow k (25 ℃) $=6.7\times10^{-5}$ s^{-1} solvolysis. Activation parameters for the oxidation step are $\Delta H^{\neq}=3.5$ kcal/mol and $\Delta S^{\neq}=-23$ eu. The geometry at ruthenium in the complex cation, $[(tpy)(bpy)Ru^{II}(OH_2)]^{2+}$, is approximately octahedral with the ligating atoms being the three N atoms of the tpy ligand, the two N atoms of the bpy ligand, and the oxygen atom of the aqua ligand. The Ru-O bond length is 2.136(5) Å.

Introduction

Metal-oxo reagents such as $KMnO_4$ or $K_2Cr_2O_7$ are useful oxidants but difficult to control in terms of product distribution. The mechanisms of these reactions are hard to unravel because of the multiple oxidation states involved.[1]

A series of polypyridyl Ru and Os mono-oxo complexes are known, which have proved to be versatile stoichiometric and/or catalytic oxidants toward a variety of organic and inorganic substrates based on $Ru^{IV/III}$ and $Ru^{III/II}$ couples.[2] The cleavage of DNA has also been reported.[3] The results of mechanistic studies based on $[(bpy)_2(py)Ru^{IV}=O]^{2+}$ (bpy is 2,2′-bipyridine and py is pyridine) as oxidant with a variety of substrates have demonstrated many reaction pathways.[4] There is far less mechanistic information available for $[(tpy)(bpy)Ru^{IV}=O]^{2+}$ as oxidant even though it is of value in catalytic reactions.[5] Reduction potentials relating its three oxidation states at pH=7 (*vs* SSCE at 22± 2 ℃) are shown in the Latimer diagram in equation 1.